Fault Tolerance for Kinematically Redundant Manipulators: Anticipating Free-Swinging Joint Failures

James D. English, *Member, IEEE,* and Anthony A. Maciejewski, *Member, IEEE*

***Abstract*—Fault tolerance is an important design criterion for robotic systems operating in hazardous or remote environments. This article addresses the issue of tolerating a free-swinging joint failure by focusing on how to best configure a slow-moving manipulator before a failure. Three scalar measures of fault susceptibility are defined using joint torques/forces, accelerations, and swing angles. Minimizing these measures is an approach to achieving fault tolerance, and for this, algorithms to calculate their gradients are also given. The formulas are valid for general n-link manipulators.**

***Index Terms*— Fault/failure tolerance, free-swinging failure, kinematics, kinematically redundant, manipulators, redundant robots/manipulators, robots.**

I. Introduction

ROBOTS that operate in remote or hazardous environments must be used in a manner that reflects the implications of failure scenarios on system performance [1]–[3]. Kinematically redundant robots have been proposed for use in such environments due to their dexterity before a failure and ability to continue operation after a failure [4]–[6]. A crucial component of any system designed to tolerate failures is the ability to detect and address different failure modes [7]. Much of this previous work has focused on failures that are modeled as locked joints, either because the failure directly results in an inability to move or because brakes are applied to prevent unpredictable behavior.

In contrast, the study of free-swinging failures is still in its infancy and presents fresh problems and additional possibilities for usefulness after a failure [8]. The term *free-swinging failure* refers to a hardware or software fault in a robotic manipulator that causes the loss of torque (or force) on a joint. Examples include a ruptured seal on a hydraulic actuator, the loss of electric power and brakes on an electric actuator, and a mechanical failure in a drive system. After a free-swinging failure, the failed joint moves freely under the influence of external forces and gravity, hence the descriptive label.

This article addresses the issue of how to best configure a slow-moving kinematically redundant manipulator in anticipation of a free-swinging failure. Manipulators used in hazardous or remote environments are typically slow moving. Kinematic redundancy allows the best configuration to be found by establishing fault tolerance as a secondary criterion to be met without affecting the end-effector task. To this end, three secondary criteria will be developed, each addressing a different aspect of a failure: torque/force, acceleration, and swing angle.

Manuscript received January 21, 1997; revised March 16, 1998. This paper was presented at the 1996 IEEE International Conference on Robotics and Automation. This work was supported by a NASA graduate student research fellowship Grant NGT9-2 and by Sandia National Laboratories under Contract AL-3011. This paper was recommended for publication by Associate Editor Y. F. Zheng and Editor A. Goldenberg upon evaluation of the reviewers' comments.

J. D. English is with Raytheon Systems Company, Tucson, AZ 85706-1151 USA.

A. A. Maciejewski is with Purdue University, West Lafayette, IN 47907-1285 USA.

Publisher Item Identifier S 1042-296X(98)04616-3.

II. A Mathematical Framework for Establishing Failure-Susceptibility Measures

The method for reducing the likelihood or negative consequences of a failure is this: A scalar measure of failure susceptibility is defined as a function of the joint variables, then it is minimized using the manipulator's kinematic redundancy. The approach to defining an overall measure will be to first establish for each joint a measure of susceptibility to a failure of *that joint alone*, then combine these in a meaningful way to form the comprehensive scalar measure.

Let $k_i(\mathbf{q})$ be the failure-susceptibility measure of joint i alone. Then, for an n-degree-of-freedom manipulator, a column of joint measures, $\mathbf{k}(\mathbf{q})$, is formed as

$$\mathbf{k}(\mathbf{q}) = [k_1 \quad k_2 \quad \cdots \quad k_n]^T. \tag{1}$$

For positive semidefinite weighting matrix $\mathbf{W}_k$, the form of the comprehensive failure-susceptibility measure f_k to be used in this work is

$$f_k(\mathbf{q}) = \mathbf{k}^T(\mathbf{q})\mathbf{W}_k\mathbf{k}(\mathbf{q}). \tag{2}$$

To reduce the effects of an impending free-swinging joint failure, f_k is minimized. Several widely known methods of optimizing secondary cost functions under the constraint of completing a primary task have been presented. The augmented-Jacobian technique [9], [10] can be used to track a desired value of the secondary criterion function. For precise tracking of critical points, the extended-Jacobian technique is appropriate [11]. And to track a local minimum or maximum,

the gradient-projection method can be used [12], [13]. These techniques require knowledge of the gradient of the function.

Application of the chain rule to (2) gives the gradient of f_k as

$$\nabla f_k = 2[D\mathbf{k}]^T \mathbf{W}_k \mathbf{k} \tag{3}$$

where

$$[D\mathbf{k}] = [\nabla k_1 \quad \nabla k_2 \quad \cdots \quad \nabla k_n]^T. \tag{4}$$

With this, ∇f_k is established as a function of the jointwise measures (k_i's) and their gradients (∇k_i's). Sections III, IV, and V to follow will develop values for the k_i's (each addressing a different failure aspect) and methods to calculate their gradients.

III. A Torque-Based Measure

In this section, a fault-susceptibility measure will be given that is based on the joint torques/forces (hereafter "joint torque" will be used to denote either torque or force for rotational or prismatic joints, respectively). A joint-torque-based measure is appropriate in that the torques at a manipulator's joints are related to both the effect and likelihood of a failure. Should joint i undergo a free-swinging failure during operation, the torque on joint i is precisely the instantaneous force-domain change induced by the failure. It is related to the joint acceleration after a failure (this relationship will be detailed in Section IV), and if it is zero the failure will have no immediate effect. Moreover, a joint under less torque is less likely to fail. (The load to induce a failure in a mechanical part is reasonably assumed to have a normal distribution [14].)

A shortcoming of the torque-based measure is that a low-torque solution may result in a large swing angle for a rotational joint after a failure. This issue will be addressed in Section V.

A. Definition of the Measure, $f_g(\mathbf{q})$

Joint torques are functions of the manipulator's motion and configuration. For a viscous friction model, this relationship is expressed mathematically as

$$\boldsymbol{\tau} = \mathbf{M}(\mathbf{q})\,\ddot{\mathbf{q}} + \mathbf{C}(\mathbf{q}, \dot{\mathbf{q}})\,\dot{\mathbf{q}} + \mathbf{V}(\mathbf{q})\dot{\mathbf{q}} + \mathbf{g}(\mathbf{q}). \tag{5}$$

Here, $\boldsymbol{\tau}$ is the vector of joint torques; $\mathbf{q}$ is the vector of joint positions; $\mathbf{M}(\mathbf{q})$ is the manipulator inertia matrix; $\mathbf{C}(\dot{\mathbf{q}}, \mathbf{q})$ is the matrix specifying centrifugal and Coriolis effects, each row i of which has the form $\dot{\mathbf{q}}^T \mathbf{C}_i(\mathbf{q})$; $\mathbf{V}(\mathbf{q})$ is the viscous-friction matrix; and $\mathbf{g}(\mathbf{q})$ is the vector of joint torques due to gravity.

Local optimization of the total torque given by (5) has been addressed [15], but it was found that this approach has regions of inherent instability [16]. The task of globally optimizing a function of the torques from (5) over a path has also been addressed [17], [18], but such global optimizations are computationally complex and not appropriate for on-line control. For a slow-moving manipulator, however, an approximation can be made that allows stable on-line optimization.

For a given robotic system, a slow moving trajectory can be defined in terms of a column vector τ_m of positive maximum torque magnitudes by requiring

$$|\boldsymbol{\tau} - \mathbf{g}| < \boldsymbol{\tau}_m \tag{6}$$

where the operations $|\cdot|$ and $<$ apply on an entry-by-entry basis. Note that (for the viscous friction model) from the dependence of $\boldsymbol{\tau} - \mathbf{g}$ on $\dot{\mathbf{q}}$ and $\ddot{\mathbf{q}}$ in (5), for any twice-differentiable joint trajectory and any τ_m, a trajectory satisfying (6) can be found simply by scaling the trajectory time.

For a sufficiently slow trajectory, the torques can be reduced to those of the static case, where $\dot{\mathbf{q}}$ and $\ddot{\mathbf{q}}$ vanish, and (5) becomes

$$\boldsymbol{\tau} = \mathbf{g}(\mathbf{q}). \tag{7}$$

This gives the vector of joint torques needed to counter gravity in a stationary manipulator, and each individual torque forms a measure through its magnitude of susceptibility to a free-swinging failure of its joint.

Using $\mathbf{k} = \mathbf{g}$ in (2) gives f_g, the scalar failure-susceptibility measure for the torque-based approach. Here $\mathbf{W}_k = \mathbf{W}_g$ is a positive semidefinite matrix that weights the relative importance of the joint torques. Example weighting matrices will be given in Section VI.

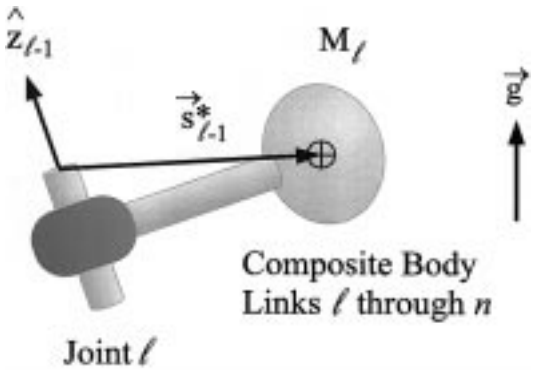

Fig. 1. Vector quantities used in calculating the torque on joint ℓ. Unit vector $\hat{z}_{\ell-1}$ is the z-axis of D-H frame $\ell - 1$. Vector $\vec{s}^*_{\ell-1}$ is the first-moment-of-inertia vector for the composite rigid body formed by links ℓ through n. Vector $\vec{g}$ is the upward-pointing gravity vector. Scalar M_ℓ is the composite mass of links ℓ through n.

B. Calculating the Gradient, ∇f_g

For $\mathbf{k} = \mathbf{g}$, (3) establishes the gradient of the overall cost function as a function of the joint torques ($\mathbf{g}$) and the torques' gradients ($D\mathbf{g}$). The remainder of this section describes a method for finding these quantities.

Joint i Rotational When joint i is rotational, the torque g_i can be calculated as

$$g_i = (\hat{z}_{i-1} \times \vec{s}^*_{i-1}) \cdot \vec{g} \tag{8}$$

where $\hat{z}_\ell$ is the unit vector along joint $\ell + 1$, the z-axis of the ℓth Denavit–Hartenberg (D-H) coordinate frame; $\vec{s}^*_\ell$ is the first moment of inertia of the composite rigid body formed by links $\ell + 1$ through n referred to the origin of D-H frame ℓ; and $\vec{g}$ is the gravity vector in the upward direction. These vector quantities are illustrated in Fig. 1.

Let M_i be the composite mass of links i through n, calculated independently of joint type as

$$M_i = m_i + M_{i+1}; \quad M_n = m_n. \tag{9}$$

Here m_i is the mass of link i. Using these values, the composite first-moment-of-inertia vector $\vec{s}_i^*$ as expressed in the ith D-H frame can be calculated independently of joint type as

$$\vec{s}_i^* = {}^i\mathbf{R}_{i+1}(\vec{s}_{i+1}^* + \vec{s}_{i+1} + M_{i+1}\vec{p}_{i\to i+1}); \ \vec{s}_n^* = \vec{0}. \tag{10}$$

Here, ${}^i\mathbf{R}_{i+1}$ is the 3×3 rotation matrix representing D-H frame $i+1$ in frame i; $\vec{s}_\ell$ is the first-moment-of-inertia vector for link ℓ referred to and expressed in its own D-H frame; and $\vec{p}_{i\to\ell}$ is the vector from the origin of D-H frame i to the origin of frame ℓ, expressed in frame ℓ. Note that m_n and $\vec{s}_n^*$ should reflect any payload that is present.

The gradient of g_i has entries $\frac{\partial g_i}{\partial q_j}$. For joint i rotational, using (8), the values of these entries are given by

$$\frac{\partial g_i}{\partial q_j} = \left(\left[\frac{\partial}{\partial q_j} \hat{z}_{i-1} \right] \times \vec{s}_{i-1}^* + \hat{z}_{i-1} \times \left[\frac{\partial}{\partial q_j} \vec{s}_{i-1}^* \right] \right) \cdot \vec{g} \tag{11}$$

provided $\frac{\partial}{\partial q_j}\hat{z}_{i-1}$ and $\frac{\partial}{\partial q_j}\vec{s}_{i-1}^*$ are found with respect to the base frame and $\vec{g}$ is constant in the base frame. This allows calculation of the gradient once the vector partial derivatives are found. Equation (11) is given in coordinate-free form, and after calculation of $\frac{\partial}{\partial q_j}\hat{z}_{i-1}$ and $\frac{\partial}{\partial q_j}\vec{s}_{i-1}^*$ it can be evaluated in any frame.

Joint i Prismatic When joint i is prismatic, the force g_i is a function only of the orientation of the joint (as compared to the dependence on the first moment of inertia when joint i is rotational). The value g_i is now given by

$$g_i = M_i \hat{z}_{i-1} \cdot \vec{g} \tag{12}$$

and the elements of the gradient are

$$\frac{\partial g_i}{\partial q_j} = M_i \left(\frac{\partial}{\partial q_j} \hat{z}_{i-1} \cdot \vec{g} \right) \tag{13}$$

provided $\frac{\partial}{\partial q_j}\hat{z}_{i-1}$ is found with respect to the base frame and $\vec{g}$ is constant in the base frame. Like (11), this can be evaluated in any frame once the vector partial derivatives are found.

C. Calculation of $\frac{\partial}{\partial q_j}\hat{z}_i$ and $\frac{\partial}{\partial q_j}\vec{s}_i^*$

The elements of ∇g_i can be calculated directly from (11) or (13) only after $\frac{\partial}{\partial q_j}\hat{z}_i$ and $\frac{\partial}{\partial q_j}\vec{s}_i^*$ have been evaluated. When joint j is rotational, $\frac{\partial}{\partial q_j}\hat{z}_i$ and $\frac{\partial}{\partial q_j}\vec{s}_i^*$ can be found in the base frame as

$$\begin{aligned} \frac{\partial}{\partial q_j}\hat{z}_i &= \hat{z}_{j-1} \times \hat{z}_i \quad j \le i \\ &= \vec{0} \qquad\qquad j > i \end{aligned} \tag{14}$$

$$\begin{aligned} \frac{\partial}{\partial q_j}\vec{s}_i^* &= \hat{z}_{j-1} \times \vec{s}_{j-1}^* \quad j > i \\ &= \hat{z}_{j-1} \times \vec{s}_i^* \qquad j \le i \end{aligned} \tag{15}$$

and when joint j is prismatic

$$\frac{\partial}{\partial q_j}\hat{z}_i = \vec{0} \tag{16}$$

$$\begin{aligned} \frac{\partial}{\partial q_j}\vec{s}_i^* &= \vec{0} \qquad\qquad j \le i \\ &= M_j \hat{z}_{j-1} \quad j > i. \end{aligned} \tag{17}$$

IV. An Acceleration-Based Measure

The last section presented a fault-susceptibility measure based on the stationary joint torques. Among the justifications for this was joint torque's relationship to joint acceleration after a failure. In this section, the jointwise function will be precisely the acceleration after a failure. Though this new measure does not have the failure-prevention properties of the torque-based approach, it relates more accurately to the immediate failure dynamics. If failed joint acceleration is low, more time is available to compensate for the failure before significant arm motion. This principle, and the method, applies to both rotational and prismatic joints. As in the torque-based case, a stationary manipulator is assumed as an approximation to a slow-moving manipulator.

A. Definition of the Measure, $f_a(\mathbf{q})$

The velocity of an inertial body cannot change instantaneously. So, at the moment of failure for a stationary manipulator, the joint rates do not change, $\dot{\mathbf{q}}$ remains $\mathbf{0}$, and (5) becomes

$$\tau = \mathbf{M}(\mathbf{q})\ddot{\mathbf{q}} + \mathbf{g}(\mathbf{q}) \tag{18}$$

where, for failed joint i

$$\tau_i = 0 \tag{19}$$

and since a stationary prefailure manipulator is assumed

$$\ddot{q}_j = 0, \quad j \ne i. \tag{20}$$

With (19) and (20), (18) gives the following scalar equation for $a_i = \ddot{q}_i$, the acceleration of the failed joint

$$0 = M_{ii}a_i + g_i \tag{21}$$

where M_{ii} is diagonal entry i of $\mathbf{M}$. Since the manipulator inertia matrix is positive definite [19], M_{ii} is strictly positive, and the following is always valid:

$$a_i = -\frac{g_i}{M_{ii}}. \tag{22}$$

With this, the column vector of joint measures is

$$\mathbf{a} = [a_1 \quad a_2 \quad \cdots \quad a_n]^T. \tag{23}$$

Using $\mathbf{k} = \mathbf{a}$ and $\mathbf{W}_k = \mathbf{W}_a$, a positive semidefinite weighting matrix, the framework of Section II establishes f_a, the scalar failure-susceptibility measure for the acceleration-based approach. Note this is an anticipatory measure (the acceleration is manifest only if a failure occurs) and not a measure of a current physical phenomenon as was the torque-based measure.

B. Calculating the Gradient, ∇f_a

With $\mathbf{k} = \mathbf{a}$, (3) allows calculation of the gradient of f_a as a function of the postfailure accelerations ($\mathbf{a}$) and their gradients ($D\mathbf{a}$).

The entries of ∇a_i (which forms row i of $D\mathbf{a}$) can be found by applying the quotient rule to (22)

$$\frac{\partial a_i}{\partial q_j} = \frac{-\frac{\partial g_i}{\partial q_j} M_{ii} + \frac{\partial M_{ii}}{\partial q_j} g_i}{M_{ii}^2}. \tag{24}$$

Equations (22) and (24) allow calculation of $\mathbf{a}$ and $D\mathbf{a}$ once M_{ii}, $\frac{\partial M_{ii}}{\partial q_j}$, g_i, and $\frac{\partial g_i}{\partial q_j}$ are known. The joint torque $\tau_i = g_i$ can be calculated using (8) for joint i rotational or (12) for joint i prismatic. The partial derivatives of g_i can be calculated using (11) for joint i rotational or (13) for joint i prismatic. This leaves M_{ii} and $\frac{\partial M_{ii}}{\partial q_j}$.

C. Calculation of the Diagonal Entries of the Mass Matrix and Their Gradients

The methods for calculating M_{ii} and $\frac{\partial M_{ii}}{\partial q_j}$ will be broken down into cases for prismatic versus rotational joints and inboard versus outboard variables for the gradients.

The Diagonal Entries When joint i is rotational, M_{ii} is given by

$$M_{ii} = \hat{z}_{i-1} \cdot \mathbf{J}^*_{i-1} \hat{z}_{i-1} \tag{25}$$

where $\mathbf{J}^*_\ell$ is the composite rigid-body inertia of links $\ell + 1$ through n referred to D-H frame ℓ. It can be calculated recursively as (adapted from [20])

$$\begin{aligned}\mathbf{J}^*_i = {}& {}^i\mathbf{R}_{i+1}(\mathbf{J}^*_{i+1} + \mathbf{J}_{i+1} - \mathbf{P}_{i\to i+1}(\mathbf{S}^*_{i+1} + \mathbf{S}_{i+1}) \\ & - (\mathbf{S}^*_{i+1} + \mathbf{S}_{i+1} + M_{i+1}\mathbf{P}_{i\to i+1})\mathbf{P}_{i\to i+1})\,{}^i\mathbf{R}^T_{i+1}\end{aligned} \tag{26}$$

$$\mathbf{J}^*_n = \mathbf{0}. \tag{27}$$

The matrix $\mathbf{S}_\ell$ is the cross-product matrix for $\vec{s}_\ell$ (the matrix such that $\mathbf{S}_\ell \vec{v} = \vec{s}_\ell \times \vec{v}$ for all vectors $\vec{v}$), $\mathbf{S}^*_\ell$ is the cross-product matrix for $\vec{s}^*_\ell$, $\mathbf{P}_{i\to\ell}$ is the cross-product matrix for $\vec{p}_{i\to\ell}$, and $\mathbf{J}_\ell$ is the second moment of inertia of link ℓ referred to its own D-H frame. Matrices without a preceding superscript are expressed in their frame of definition (ℓ for $\mathbf{J}_\ell$, $\mathbf{J}^*_\ell$, $\mathbf{S}_\ell$, $\mathbf{S}^*_\ell$, and $\mathbf{P}_{i\to\ell}$). Note that $\mathbf{J}_n$ should reflect any payload that is present.

When joint i is prismatic, M_{ii} is simply the composite mass of links i through n; i.e.,

$$M_{ii} = M_i \tag{28}$$

with the composite mass M_i calculated using (9).

The Gradients For joints i and j rotational, $i < j$, from (25)

$$\frac{\partial M_{ii}}{\partial q_j} = \hat{z}_{i-1} \cdot \frac{\partial}{\partial q_j} \mathbf{J}^*_{i-1} \hat{z}_{i-1} \tag{29}$$

where the fact that $\hat{z}_{i-1}$ is inboard from q_j and therefore does not change with q_j was used. Taking the partial derivative of $\mathbf{J}^*_{i-1}$ with respect to q_j gives, in coordinate-free form

$$\begin{aligned}&\frac{\partial}{\partial q_j}\mathbf{J}^*_{i-1} \\ &\quad = \mathbf{Z}_{j-1}\mathbf{J}^*_{j-1} + \mathbf{P}_{i-1\to j-1}(\mathbf{S}^*_{j-1}\mathbf{Z}_{j-1} - \mathbf{Z}_{j-1}\mathbf{S}^*_{j-1}) \\ &\qquad - \mathbf{J}^*_{j-1}\mathbf{Z}_{j-1} + (\mathbf{S}^*_{j-1}\mathbf{Z}_{j-1} - \mathbf{Z}_{j-1}\mathbf{S}^*_{j-1})\mathbf{P}_{i-1\to j-1}\end{aligned} \tag{30}$$

where $\mathbf{Z}_\ell$ is the cross-product matrix for $\hat{z}_\ell$. Substituting (30) into (29), exploiting the symmetry of $\mathbf{J}^*_{j-1}$, and simplifying gives

$$\begin{aligned}&\frac{\partial M_{ii}}{\partial q_j} \\ &\quad = 2(\hat{z}_{i-1} \times \vec{p}_{(i-1)\to(j-1)} \cdot (\vec{s}^*_{j-1} \times (\hat{z}_{j-1} \times \hat{z}_{i-1}) \\ &\qquad - \hat{z}_{j-1} \times (\vec{s}^*_{j-1} \times \hat{z}_{i-1})) + (\hat{z}_{i-1} \times \hat{z}_{j-1}) \cdot \mathbf{J}^*_{j-1}\hat{z}_{i-1}).\end{aligned} \tag{31}$$

This can be efficiently calculated in frame $j - 1$.

For joint i rotational and joint j prismatic, $i < j$, taking the partial derivative of $\mathbf{J}^*_{i-1}$ with respect to q_j (now a sliding variable) gives, in coordinate-free form

$$\frac{\partial}{\partial q_j}\mathbf{J}^*_{i-1} = -\mathbf{P}_{i-1\to j-1}\left[\frac{\partial}{\partial q_j}\mathbf{S}^*_{j-1}\right] - \left[\frac{\partial}{\partial q_j}\mathbf{S}^*_{j-1}\right]\mathbf{P}_{i-1\to j-1}. \tag{32}$$

Using $\frac{\partial}{\partial q_j}\mathbf{S}^*_{j-1} = M_j\mathbf{Z}_{j-1}$ with (32) in (29), which is valid for all types of joint j, gives

$$\frac{\partial M_{ii}}{\partial q_j} = 2M_j(\hat{z}_{i-1} \times \hat{z}_{j-1}) \cdot (\hat{z}_{i-1} \times \vec{p}_{(i-1)\to(j-1)}) \tag{33}$$

which can be efficiently calculated in frame $j - 1$.

For joint i rotational and joint j either prismatic or rotational, $i \geq j$, M_{ii} is constant for changing q_j, and thus

$$\frac{\partial M_{ii}}{\partial q_j} = 0. \tag{34}$$

For prismatic joint i, all j, the composite mass of links i through n is not changed by the value of joint variable j, and thus, from (28)

$$\frac{\partial M_{ii}}{\partial q_j} = 0. \tag{35}$$

V. A Swing-Angle-Based Measure

In this section, the failure-susceptibility measure will be based on the angle through which a failed rotational joint moves after a failure, that is, the angle between the prefailure configuration and the settled, postfailure configuration. This is defined as the swing angle. When it is small, a failure will produce a displacement that will, in a relative sense, be small, and when it is zero, a failure will have no effect (for the given assumptions). The expectation is that with a small swing angle, the manipulator is less likely to cause secondary damage to itself or its environment. This measure is for rotational joints only (prismatic joints do not settle through friction, but hit stops), and, again, a stationary manipulator is assumed as an approximation to a slow moving one.

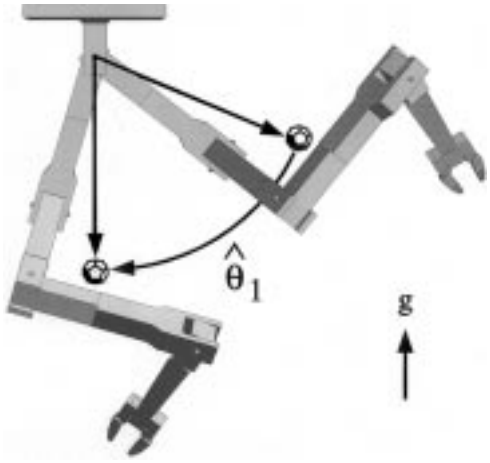

Fig. 2. The swing angle for joint one, $\hat{\theta}_1$. Shown here is a manipulator before (upper right) and after (lower) a failure of the first joint. The center of mass of the manipulator is represented by the small polyhedron.

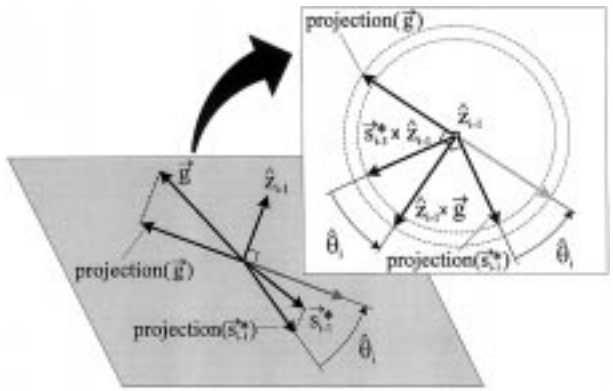

Fig. 3. The swing angle is the angle between the projection of $\vec{s}^{\,*}_{i-1}$ and the negative of the projection of $\vec{g}$. It is equal to the angle between $\vec{s}^{\,*}_{i-1} \times \hat{z}_{i-1}$ and $\hat{z}_{i-1} \times \vec{g}$.

If the environment is well known, configuration-space analysis of the workspace could be used to specify a range of swing angles that would not induce collision. No assumptions about the environment, however, are made for this work, and the approach will be to reduce the magnitude of the swing angles. A shortcoming of a swing-angle based measure is that it provides a limited amount of information on the Cartesian motion of the manipulator [21].

A. Definition of the Measure, $f_{\hat{\theta}}(\mathbf{q})$

The swing angle $\hat{\theta}_i$ is the angle through which failed joint i moves to find its resting position after a failure. The resting position is that for which the center of mass of the portion of the manipulator outboard from the failed joint is at its lowest position relative to the gravitational field. This is illustrated for a failure of the base joint in Fig. 2.

With the definitions of $\hat{z}_\ell, \vec{s}^{\,*}_\ell$, and $\vec{g}$ as given in Section III, the angle through which joint i would swing were it to fail is given by the angle between the projections of $\vec{s}^{\,*}_{i-1}$ and $-\vec{g}$ onto the plane perpendicular to $\hat{z}_{i-1}$ (the axis of rotation). This can be calculated as the angle between $(\vec{s}^{\,*}_{i-1} \times \hat{z}_{i-1})$ and $(\hat{z}_{i-1} \times \vec{g})$, as shown in Fig. 3; i.e.,

$$\cos(\hat{\theta}_i) = \frac{(\vec{s}^{\,*}_{i-1} \times \hat{z}_{i-1}) \cdot (\hat{z}_{i-1} \times \vec{g})}{||\vec{s}^{\,*}_{i-1} \times \hat{z}_{i-1}||||\hat{z}_{i-1} \times \vec{g}||} \tag{36}$$

$$\sin(\hat{\theta}_i) = \frac{\hat{z}_{i-1} \cdot (\vec{g} \times \vec{s}^{\,*}_{i-1})}{||\vec{s}^{\,*}_{i-1} \times \hat{z}_{i-1}||||\hat{z}_{i-1} \times \vec{g}||}. \tag{37}$$

Provided neither $\vec{s}^{\,*}_{i-1}$ nor $\vec{g}$ is parallel to $\hat{z}_{i-1}$, (36) and (37) give

$$\hat{\theta}_i = \mathrm{Atan2}[\hat{z}_{i-1} \cdot (\vec{g} \times \vec{s}^{\,*}_{i-1}), (\vec{s}^{\,*}_{i-1} \times \hat{z}_{i-1}) \cdot (\hat{z}_{i-1} \times \vec{g})] \tag{38}$$

where the range of Atan2 is $-\pi$ to π; otherwise, from (8), the torque on joint i is zero, and since a stationary manipulator is assumed

$$\hat{\theta}_i = 0. \tag{39}$$

The jointwise measure for use within the framework established in Section II will be the swing angle. The column vector of joint measures will be given by

$$\hat{\theta} = [\hat{\theta}_1 \quad \hat{\theta}_2 \quad \cdots \quad \hat{\theta}_n]^T. \tag{40}$$

Using $\mathbf{k} = \hat{\theta}$ and $\mathbf{W}_k = \mathbf{W}_{\hat{\theta}}$, a positive semidefinite weighting matrix, the framework of Section II establishes $f_{\hat{\theta}}$, the scalar failure-susceptibility measure for the swing-angle-based approach.

B. Calculating the Gradient, $\nabla f_{\hat{\theta}}$

The gradient of $f_{\hat{\theta}}$ can be calculated using (3), which, for $\mathbf{k} = \hat{\theta}$, establishes the gradient of the measure as a function of the swing angles $(\hat{\theta})$ and their gradients $(D\hat{\theta})$.

If $\vec{s}^{\,*}_{i-1}$ or $\vec{g}$ is parallel to $\hat{z}_{i-1}$, the gradient of $\hat{\theta}_i$ is either $\mathbf{0}$ or undefined and should be set to $\mathbf{0}$. Otherwise, from (38), the entries of $\nabla\hat{\theta}_i$ are calculated as

$$\frac{\partial\hat{\theta}_i}{\partial q_j} = \frac{1}{u_{i,1}^2 + u_{i,2}^2}\left(\frac{\partial u_{i,1}}{\partial q_j}u_{i,2} - \frac{\partial u_{i,2}}{\partial q_j}u_{i,1}\right) \tag{41}$$

where

$$u_{i,1} = \hat{z}_{i-1} \cdot (\vec{g} \times \vec{s}^{\,*}_{i-1}) \tag{42}$$

and

$$u_{i,2} = (\vec{s}^{\,*}_{i-1} \times \hat{z}_{i-1}) \cdot (\hat{z}_{i-1} \times \vec{g}). \tag{43}$$

Equation (41) is valid for all values of $\hat{\theta}_i$ between $-\pi$ and π.

C. Calculation of $\frac{\partial}{\partial q_j}u_{i,1}$ and $\frac{\partial}{\partial q_j}u_{i,2}$

When all vector quantities are expressed in the base frame and the gravity vector there is constant, (42) and (43) give

$$\frac{\partial u_{i,1}}{\partial q_j} = \frac{\partial}{\partial q_j}\hat{z}_{i-1}\cdot(\vec{g}\times\vec{s}^{*}_{i-1}) + \hat{z}_{i-1}\cdot\left(\vec{g}\times\frac{\partial}{\partial q_j}\vec{s}^{*}_{i-1}\right) \quad (44)$$

and

$$\frac{\partial u_{i,2}}{\partial q_j} = \left(\frac{\partial}{\partial q_j}\vec{s}^{*}_{i-1}\times\hat{z}_{i-1} + \vec{s}^{*}_{i-1}\times\frac{\partial}{\partial q_j}\hat{z}_{i-1}\right)\cdot(\hat{z}_{i-1}\times\vec{g}) + (\vec{s}^{*}_{i-1}\times\hat{z}_{i-1})\cdot\left(\frac{\partial}{\partial q_j}\hat{z}_{i-1}\times\vec{g}\right) \quad (45)$$

where $\frac{\partial}{\partial q_j}\hat{z}_{i-1}$ and $\frac{\partial}{\partial q_j}\vec{s}^{*}_{i-1}$ can be calculated using (14), (15), (16), and (17).

VI. Examples

To illustrate the concepts of this article, two examples will be given using a three-link planar manipulator. Hardware experiments using a seven-link manipulator will then be presented to demonstrate the applicability to spatial arms.

A. A Torque-Based Multi-Joint Example

The example planar manipulator used here is described as follows: the link lengths are unity; the link masses are unity; and the center of mass of each link is at the link center. The task will be end-effector positioning only (i.e., orientation is not considered), and with this perspective, the manipulator has one degree of kinematic redundancy.

For this first example, a free-swinging failure is anticipated at any joint, and the torque-based method will be used. Values for $\mathbf{W}_g$ will be determined by analyzing the worst-case stationary joint torques. When the manipulator is fully extended horizontally, the gravitational torques on joints one, two, and three are at their global maximums of $\frac{9g}{2}$, $\frac{4g}{2}$, and $\frac{g}{2}$, respectively, where g is the magnitude of the acceleration due to gravity. If the actuators are designed to be capable of applying torque proportional to this worst case, then for the purpose of failure prevention, the ratio of the applied torque to the maximum is of concern. These are found by weighting joint-one torque by $\frac{2}{9g}$, joint-two torque by $\frac{2}{4g}$, and joint-three torque by $\frac{2}{g}$. This gives, after normalizing

$$\mathbf{W}_g = \begin{bmatrix} \frac{1}{81} & 0 & 0 \\ 0 & \frac{1}{16} & 0 \\ 0 & 0 & 1 \end{bmatrix}. \quad (46)$$

For this value of $\mathbf{W}_g$ used as a weighting matrix in (2), worst-case and best-case configurations for end-effector position (.6, -1.9) are shown in Fig. 4. The worst-case configuration has high relative joint-two and joint-three torque, while the best-case configuration has low relative torques on all three joints.

Using the measure defined through (46) over a linear trajectory gave the results of Fig. 5. The method reduced the relative torques over the path, as is most visibly demonstrated for joint three, corresponding to the weakest actuator (the last link is near vertical over the path). The worst-case criterion function over the path is 38% of the global maximum. The asymmetry of the cost-function plot is due to the fact that a local minimum, not a global minimum, is being tracked. Any trajectory point (x, y) has an optimal configuration at least as good as that of the mirror trajectory point $(-x, y)$—the solutions over the right half of the trajectory are of better quality than the solutions over the left half.

The displacement of the joints over the path of Fig. 5 is relatively high, illustrating how reducing joint torque tends to come at a cost of increased joint displacement. In cases where displacement-induced wear and failure are of concern, an optimization based on both the torque-based criterion function and joint rates could be used, employing, for example, Liégeois's method [12]. Note, however, that in marginal lubrication-deficient cases—where failure-prevention methods

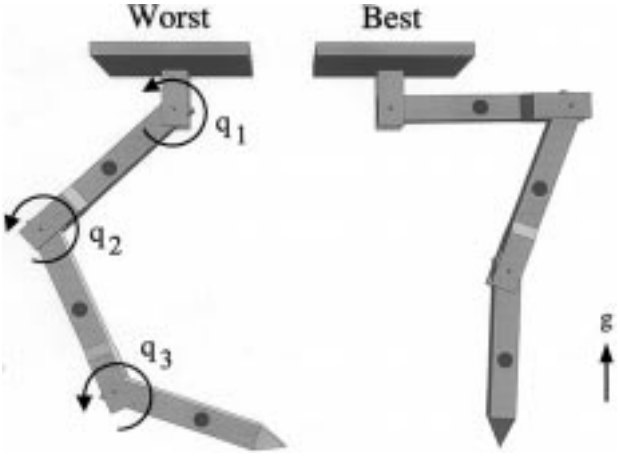

Fig. 4. The worst-case (left) and best-case (right) configurations for a stationary three-link planar revolute manipulator for prevention of a failure in any joint. The manipulator on the left has the largest cost-function value using $\mathbf{W}_g$ as given in (46) for end-effector position (.6, -1.9), and the manipulator on the right has the smallest.

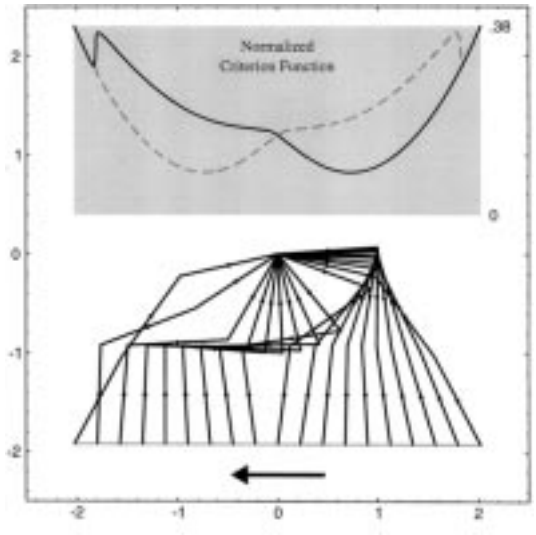

Fig. 5. Following a horizontal trajectory from right to left while minimizing the susceptibility of a failure on any joint. The normalized (globally largest value = 1) value of the cost function, based on the value of $\mathbf{W}_g$ given in (46), is plotted in the gray region versus the x-coordinate of the end effector. The gray dashed line corresponds to the criterion function plot that would result were the trajectory traversed from left to right.

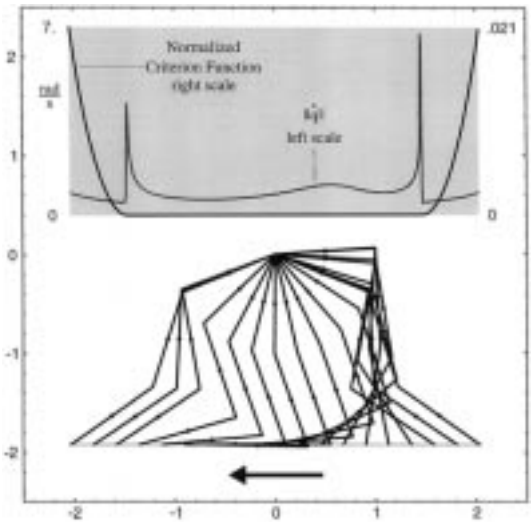

Fig. 6. Following a horizontal trajectory from right to left while minimizing the joint-two swing-angle-based measure. The normalized value of the criterion function (the joint-two swing angle squared) and the joint-rate norm (for a 10 s constant-velocity trajectory) are plotted in the gray region versus the x-coordinate of the end effector.

might be invoked—a modest reduction in load can reduce the ratio of mechanical wear to displacement by several orders of magnitude [22].

B. Swing-Angle-Based Single-Joint Example

Focusing on the joint-two swing angle, using

$$\mathbf{W}_a = \begin{bmatrix} 0 & 0 & 0 \\ 0 & 1 & 0 \\ 0 & 0 & 0 \end{bmatrix} \tag{47}$$

as a weighting matrix, over a linear trajectory gave the results of Fig. 6. The cost-function was zero over most of the trajectory, and where zero was not achievable, the joint-two swing-angle magnitude was minimized, as is evidenced by the tendency of the last two links to stay under the second joint. Had joint two failed while the arm slowly traversed the trajectory, the deviation of the arm from the desired path would have been small—the worst-case criterion function value is 2.1% of its global maximum.

Also in Fig. 6, the joint-rate norm is plotted versus the end-effector x-coordinate for a 10 s constant-velocity trajectory, and the spikes show that the manipulator experiences rapid motion at two points along the path. These points correspond to occurrences of algorithmic singularities—the manipulator's configuration at these points is not a differentiable function of end-effector position under minimizing control. The nature of the failure-susceptibility measure at and near the right-hand point is detailed in Fig. 7. When the rank of $\mathbf{W}_k$ equals the degree of redundancy (as is the case here), either an algorithmic or a kinematic singularity will always occur upon entering or leaving a region where the criterion function can be zero, provided the jointwise functions have continuous second-order derivatives within a neighborhood of the crossing minimum. A proof of this is given in [23].

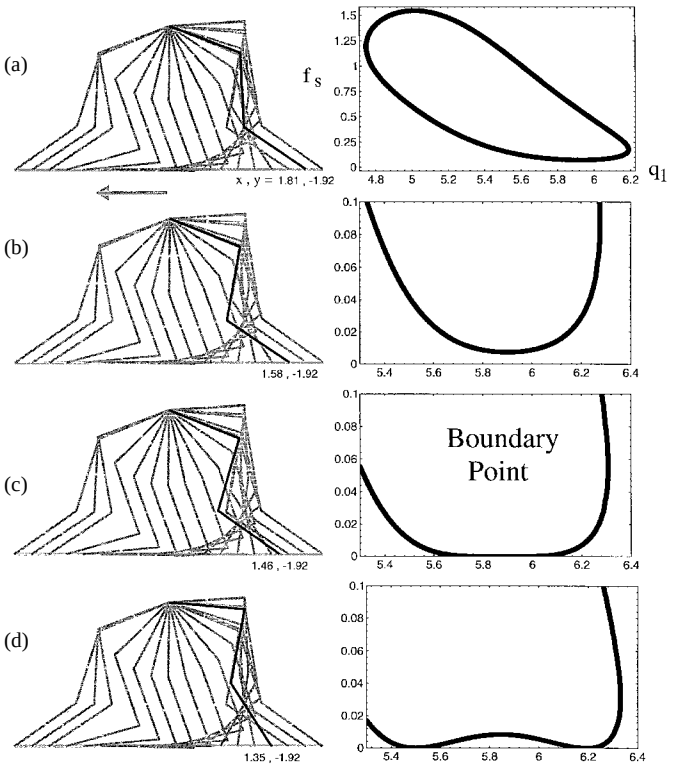

Fig. 7. An illustration of the splitting-local-minimum phenomenon based on the joint-two swing-angle-based measure. The manipulator is following a horizontal trajectory while locally minimizing the swing-angle-based measure (the same joint path as in Fig. 6). Four plots are shown of the swing-angle-based criterion function versus the first joint angle in radians (measured from horizontal) for configurations giving a desired end point. Each plot corresponds to the end point of the black arm to its left. The first plot (a) shows the range of all possible values, while the second through fourth (b)–(d) plots show a subset. The local minimum is well defined in plots one and two, but becomes poorly defined in plot three, with the end effector at the boundary of the zero-criterion-function region—the system experiences an algorithmic singularity at this point. In the fourth plot, the minimum has split (the black arm corresponds to the right-hand minimum), and the end-effector is now well within the zero-criterion-function region of the workspace

Rapid manipulator motion is undesirable and voids the slow-moving assumption. Scaling the trajectory time (i.e., reducing the end-effector trajectory speed) could prevent this [24], but if constant velocity is desired, a solution is to restrict null-space motion to reduce the joint rates without sacrificing end-effector velocity tracking. The result of this approach is shown in Fig. 8. Capping the joint rates had only a minor effect on the joint values and criterion function and did not change the end-effector trajectory. If error in the task were permissible, a damped-least-squares type of solution could also be used to limit the joint velocity.

C. Hardware Experiments

To verify the assumptions used in the development of the algorithms, hardware experiments were performed on a Robotics Research Corporation K-1207i manipulator. The K-1207i has seven joints and therefore has one degree of kinematic redundancy for the task of spatial positioning and orienting. The kinematic and dynamic parameters and joint limits for the K-1207i are given in [23]. This arm was used to verify the joint-torque-based method by tracing a linear

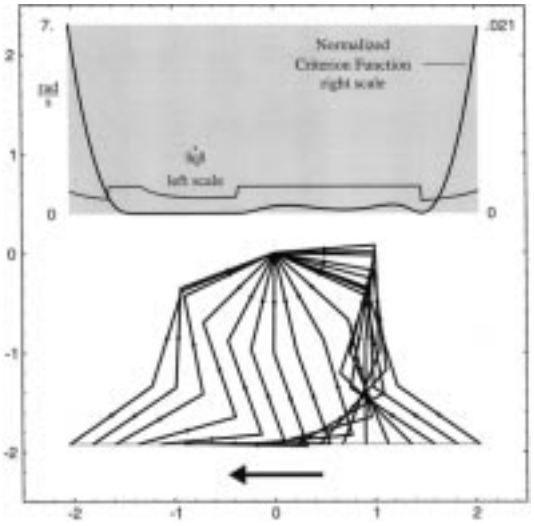

Fig. 8. Following the same horizontal trajectory as in Fig. 6 under the constraint that the joint-rate norm not exceed one radian/s. Rapid motion is avoided, yet the criterion function remains low.

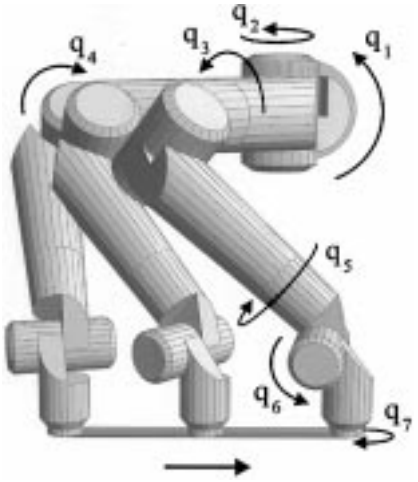

Fig. 9. The K-1207i tracing the example trajectory from left to right while locally minimizing the joint-two torque squared. The gravity vector points toward the top of the page. The second joint is aligned vertically so, independent of the configuration of the outboard joints, it has zero gravitational torque.

trajectory while minimizing the torques squared on several different joints. The case of a focus on joint two will be presented here, and the results for other joints are given in [23].

The end-effector trajectory begins with a hand pose given by the following homogeneous transformation matrix relative to the base frame

$$\mathbf{H} = \begin{bmatrix} 0 & 0 & -1 & -0.678 \\ 0 & 1 & 0 & 0.60 \\ 1 & 0 & 0 & 0.65 \\ 0 & 0 & 0 & 1 \end{bmatrix}. \tag{48}$$

The end effector then travels in the negative y-direction without rotating and ends with a pose given by

$$\mathbf{H} = \begin{bmatrix} 0 & 0 & -1 & -0.678 \\ 0 & 1 & 0 & 0 \\ 1 & 0 & 0 & 0.65 \\ 0 & 0 & 0 & 1 \end{bmatrix}. \tag{49}$$

A trapezoidal velocity profile was used to assign motion along this path. Of the total trajectory time, the first 20% was used to accelerate to the maximum speed and the last 20% was used to decelerate to a stop.

To focus on the second joint, the weighting matrix $\mathbf{W}_g$ was set to a 7×7 matrix with a 1 at position (2, 2) and zeros elsewhere. The gradient-projection technique was then used to track a local minimum along the example trajectory, and three images of the arm along this path are shown in Fig. 9. The minimization procedure here has a clear physical interpretation: it aligns the second joint with the gravitational field. With this, the model has no joint-two gravitational torque regardless of the configuration of the outboard links over the entire trajectory. This shows an optimization mechanism useful for spatial manipulators that is not available in the planar case—the reorienting of the focus joint.

The measured torques on the K-1207i's second joint in following the path of Fig. 9 are shown in Fig. 10 for three trajectory times. Because the second joint is aligned with $\vec{g}$

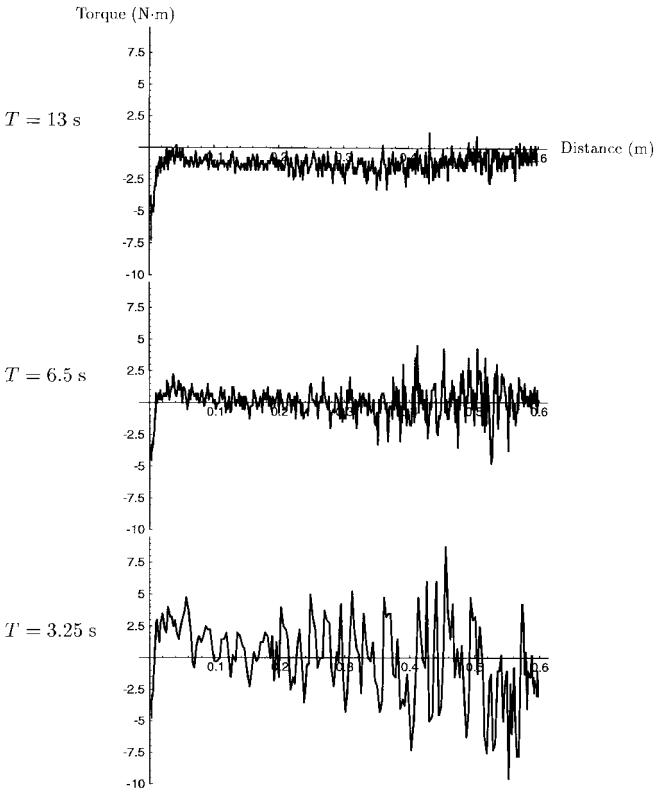

Fig. 10. Measured joint-two torque on the K-1207i versus distance along the end-effector trajectory as the arm locally minimizes the second joint torque squared (as shown in Fig. 9). The trajectory time T is halved with each subsequent plot.

along the trajectory, the dynamic torques dominate, as can be seen through the difference in the magnitudes of the torques for the $T = 3.25$ s case versus the $T = 13$ s case. The visible oscillations are due to the controller action. Yet even with these dynamic torques, the magnitude of the total joint torque is significantly reduced from what it potentially could be over the trajectory. The arm tracking a local *maximum*—under joint-

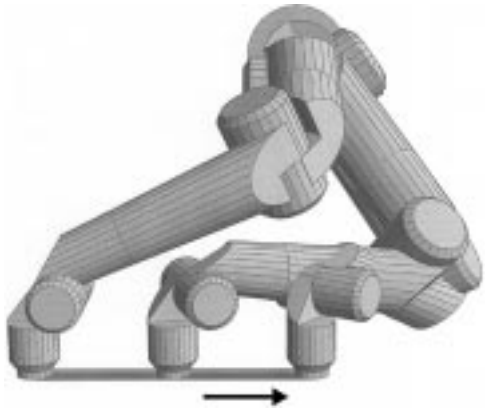

Fig. 11. The K-1207i tracing the example trajectory from left to right while locally maximizing the joint-two torque squared. The gravity vector points toward the top of the page.

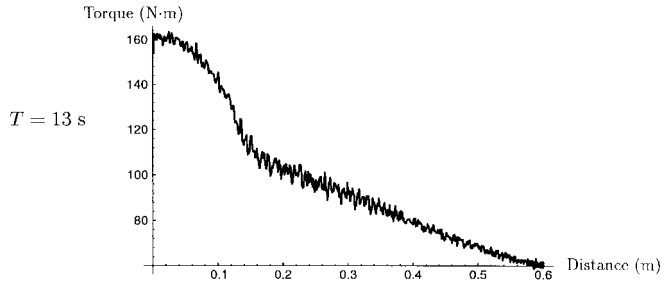

Fig. 12. Measured joint-two torque on the K-1207i versus distance along the example trajectory while maximizing the second joint torque squared (Fig. 11). The trajectory time T is 13 s. This torque magnitude is much higher than for the trajectories of Fig. 10, showing the benefit of the technique for a real system.

limit constraints—of the joint-two gravitational torque squared is shown in Fig. 11, and the resulting measured torque for a 13 s trajectory time is shown in Fig. 12. For this example, minimizing the gravitational torque dramatically reduces the total torque even for a fast trajectory time. This demonstrates the merit of the stationary-manipulator assumption.

VII. Conclusion

This article defined three cost functions which quantitatively reflected the susceptibility of a manipulator to a free-swinging joint failure:

1) the torque-based function measured failure likelihood and force-domain effects;
2) the acceleration-based function measured immediate failure dynamics; and
3) the swing-angle-based function measured susceptibility to secondary damage after a failure.

For use in minimization methods, algorithms were given for calculating the gradient of each cost function for a general spatial manipulator. These were used with the gradient-projection technique to show the methods' usefulness for a three-link planar manipulator and demonstrate the concept's practicality for a commercial seven-link manipulator.

The three measures presented address diverse aspects of a robotic system's susceptibility to a failure. They can be used independently or together. When employed to control the motion of manipulators in remote or hazardous environments, they have the potential to reduce the likelihood and negative consequences of a failure and thereby expand the general usefulness of robotic manipulators.

Acknowledgment

The authors would like to thank J. Carvajal and T. Nguyen for their useful suggestions and help in implementing the hardware experiments on the K-1207i manipulator at NASA Johnson Space Center.

References

[1] B. Christensen, W. Drotning, and S. Thunborg, "Model-based, sensor-directed remediation of underground storage tanks," *J. Robot. Syst.*, vol. 9, no. 2, pp. 145–159, 1992.
[2] R. Colbaugh and M. Jamshidi, "Robot manipulator control for hazardous waste-handling applications," *J. Robot. Syst.*, vol. 9, no. 2, pp. 215–250, 1992.
[3] E. Wu, J. Hwang, and J. Chladek, "Fault tolerant joint development for the space shuttle remote manipulator system: Analysis and experiment," in *Proc. 4th Int. Symp. Robot. Manufact. (ISRAM'92)*, Sante Fe, NM, Nov. 11–13, 1992, pp. 505–510.
[4] A. A. Maciejewski, "Fault tolerant properties of kinematically redundant manipulators," in *Proc. 1990 Int. Conf. Robot. Automat.*, Cincinnati, OH, May 13–18, 1990, pp. 638–642.
[5] C. J. J. Paredis, W. K. F. Au, and P. K. Khosla, "Kinematic design of fault tolerant manipulators," *Comput. Electric. Eng.*, vol. 20, no. 3, pp. 211–220, May 1994.
[6] C. L. Lewis and A. A. Maciejewski, "Dexterity optimization of kinematically redundant manipulators in the presence of failures," *Comput. Electric. Eng.*, vol. 20, no. 3, pp. 273–288, May 1994.
[7] M. L. Visinsky, J. R. Cavallaro, and I. D. Walker, "A dynamic fault tolerance framework for remote robots," *IEEE Trans. Robot. Automat.*, vol. 11, pp. 477–490, Aug. 1995.
[8] H. Arai and S. Tachi, "Position control of a manipulator with passive joints using dynamic coupling," *IEEE Trans. Robot. Automat.*, vol. 7, pp. 528–534, 1991.
[9] O. Egeland, "Task-space tracking with redundant manipulators," *IEEE J. Robot. Automat.*, vol. RA-3, pp. 471–475, Oct. 1987.
[10] H. Seraji, "Configuration control of redundant manipulators: Theory and implementation," *IEEE Trans. Robot. Automat.*, vol. 5, pp. 472–490, Aug. 1989.
[11] J. Baillieul, "Kinematic programming alternatives for redundant manipulators," in *Proc. 1985 Int. Conf. Robot. Automat.*, St. Louis, MO, Mar. 25–28, 1985, pp. 722–728.
[12] A. Liégeois, "Automatic supervisory control of the configuration and behavior of multibody mechanisms," *IEEE Trans. Syst., Man, Cybern.*, vol. SMC-7, pp. 868–871, Dec. 1977.
[13] C. A. Klein and C. H. Huang, "Review of pseudoinverse control for use with kinematically redundant manipulators," *IEEE Trans. Syst., Man, Cybern.*, vol. SMC-13, pp. 245–250, Mar./Apr. 1983.
[14] R. C. Johnson, "Optimum design of mechanical elements," *Factor of Safety in Design*. New York: Wiley, 1980, ch. 5, pp. 145–177.
[15] J. M. Hollerbach and K. C. Suh, "Redundancy resolution of manipulators through torque optimization," *IEEE J. Robot. Automat.*, vol. RA-3, pp. 308–316, Aug. 1987.
[16] A. A. Maciejewski, "Kinetic limitations on the use of redundancy in robotic manipulators," *IEEE Trans. Robot. Automat.*, vol. 7, pp. 205–210, Apr. 1991.
[17] K. C. Suh and J. M. Hollerbach, "Local versus global torque optimization of redundant manipulators," in *Proc. 1987 Int. Conf. Robot. Automat.*, Raleigh, NC, Mar. 31–Apr. 3, 1987, pp. 619–624.
[18] Y. Nakamura and H. Hanafusa, "Optimal redundancy control of robot manipulators," *Int. J. Robot. Res.*, vol. 6, no. 1, pp. 32–42, Spring 1987.
[19] L. T. Wang and B. Ravani, "Recursive computations of kinematic and dynamic equations for mechanical manipulators," *IEEE J. Robot. Automat.*, vol. RA-2, pp. 124–131, Sept. 1985.
[20] A. Fijany and A. K. Bejczy, "An efficient algorithm for computation of manipulator inertia matrix," *J. Robot. Syst.*, vol. 7, no. 1, pp. 57–80, 1990.

[21] J. D. English and A. A. Maciejewski, "Euclidean-space measures of robotic joint failures," in *Proc. 1997 Int. Conf. Robot. Automat.*, Albuquerque, NM, Apr. 20–25, 1997.
[22] C. N. Rowe, "Lubricated wear," in *Wear Control Handbook*, M. B. Peterson and W. O. Winer, Eds. New York: American Society of Mechanical Engineers, 1980, pp. 143–160.
[23] J. D. English, "Free-swinging failure tolerance for robotic manipulators," Ph.D. dissertation, Purdue Univ., West Lafayette, IN, 1996.
[24] J. M. Hollerbach, "Dynamic scaling of manipulator trajectories," *ASME J. Dyn. Syst., Meas., Contr.*, vol. 106, pp. 102–106, Mar. 1984.

James D. English (M'98) received the B.S. degree from the Virginia Polytechnic Institute and State University, Blacksburg, in 1988, the M.E. degree from the University of Florida, Gainesville, in 1991, and the Ph.D. degree from Purdue University, West Lafayette, IN, in 1996, all in electrical engineering.

From 1989 to 1990, he worked for the Center for Mathematical System Theory, University of Florida. From 1992 to 1993, he worked for the Voice of America, Washington, DC, and Tangier, Morocco. Since 1997, he has worked for the Raytheon Systems Company, Tucson, AZ. His primary research interests lie in the simulation and design of remote automatic systems.

Anthony A. Maciejewski (S'82–M'87) received the B.S.E.E., M.S., and Ph.D. degrees in electrical engineering from The Ohio State University, Columbus, in 1982, 1984, and 1987, respectively.

He is a Professor at the School of Electrical and Computer Engineering, Purdue University, West Lafayette, IN. His primary research interests center on the simulation and control of kinematically redundant robotic systems.